FISEVIER

Contents lists available at ScienceDirect

Journal of Analytical and Applied Pyrolysis

journal homepage: www.elsevier.com/locate/jaap



Fate of polymer derived SiC monolith at different high temperatures

Rahul Ananda, Kathy Lua, b, *

- ^a Department of Materials Science and Engineering, Virginia Tech, 260 Holden Hall, Blacksburg, VA 24061, USA
- b Department of Mechanical and Materials Engineering, EEC building 257, University of Alabama at Birmingham, Birmingham, AL 35294, USA

ARTICLE INFO

Keywords:
Polymer derived ceramics
SiC
Phase
Microstructure
High temperature

ABSTRACT

Monolithic polymer-derived SiC is highly desirable for high temperature applications because of its unique thermal properties in extreme conditions. The current study focuses on the formation, evolution, and stability of polymer-derived SiC at different high temperatures. SiC-based monoliths were pre-pyrolyzed at 1200 °C and then pyrolyzed at 1600 - 2500 °C in a flowing argon atmosphere. The porosity, density, compositions, and phases of the SiC samples were studied. Dense SiC monolith was obtained from 1200 °C to 2200 °C. SiC crystallized at 1900 °C and formed a near stoichiometric composition. β -SiC remained stable even at 2200 °C. However, the SiC monolith experienced continuous mass loss above 1900 °C and disintegrated at 2500 °C with \sim 89.5% mass loss. This work opens a pathway for preparing near stoichiometric and dense SiC monoliths through polymer precursor pyrolysis; it also provides fundamental understanding of polymer-derived SiC at different high temperatures.

1. Introduction

SiC is an important non-oxide ceramic with diverse applications due to its excellent mechanical strength, high hardness, desirable chemical and thermal stability, high melting point, good oxidation resistance, high erosion resistance, and excellent thermal shock resistance. [1] However, the covalent bonding and non-melting nature make it difficult to process by conventional methods. [2] One solution is to use polycarbosilanes for pyrolysis because of the desirable solubility in organic solvents, crosslinkability, moldability, spinnability, and high yield after pyrolysis from different preceramic precursors. [3,4].

The polycarbosilane precursor developed by Yajima et al. was the first commercially available precursor for SiC ceramics. [5] However, the O-containing curing step led to reduced long-term stability for the resulting SiC ceramic fibers. In addition, as the C/Si ratio in the precursor was 2:1, excess C was also generated after pyrolysis. This excess C has negative effects on the mechanical strength and high temperature stability of the targeted SiC fibers. [6].

Researchers have since developed better methods for producing SiC ceramics with reduced O and C contents. [7] This resulted in SiC ceramics with improved long-term stability and reduced impurities. [8] Various techniques were employed for the fabrication of high-density SiC materials. [9] One of these involves pressureless solid-state sintering, which, however, produces porous SiC parts. [10] Even though use of sintering aids such as B and C yields components with excellent resistance to high-temperature creep and oxidation, it does come with the

drawback of reduced fracture toughness. [11] Precursor infiltration and pyrolysis (PIP), technically a polymer-derived process, helps to achieve denser SiC without use of sintering aids; however, this multistep process is time consuming and costly. [9,12] Some pores cannot be removed by PIP and C may be undesirably introduced into the system. For a porous SiC material, PIP after 4 cycles and pyrolysis at 1700 °C reduced porosity from \sim 22.42 vol% to \sim 7.87 vol%. [12].

Polymer derived ceramic route addresses all the above-mentioned issues but fabrication of dense SiC using polymers is rather challenging. A wide range of precursors has been studied for the fabrication of SiC ceramics. [6,13-19] Often, there is an excessive amount of C in polymer derived SiC. [12,14] Off-stoichiometric distributions, mixed carbide phases, or mixed amorphous and crystalline phases are common issues in different polymer derived SiC. [20,21] An allylhydridopolycarbosilane (AHPCS) has been considered the best precursor to achieve a near stoichiometric SiC ceramic at high pyrolysis temperatures. Several studies have characterized AHPCS-derived SiC. [7,8,12,20,22] There have been continuous efforts to understand and improve polycarbosilanederived SiC, such as on achieving a high ceramic yield, 1:1 C/Si ratio, and bulk shapes. [23] At ultrahigh temperatures (≥1900 °C), the composition and microstructure continue to evolve, which has not been studied up to a sufficiently high temperature. The thermal limit of precursor derived SiC ceramic in extreme temperature conditions remains unknown. Understanding the behavior of SiC at ultrahigh temperatures is essential for various high-temperature applications, including ad-

https://doi.org/10.1016/j.jaap.2024.106386

Received 28 October 2023; Received in revised form 28 December 2023; Accepted 31 January 2024 0165-2370/© 20XX

Corresponding author at: Department of Materials Science and Engineering, Virginia Tech, 260 Holden Hall, Blacksburg, VA, 24061, USA.
 E-mail address: klu@uab.edu (K. Lu).

vanced structural ceramics, high-temperature electronics, and specialized coatings.

The current study addresses the above issues related to the fabrication of dense monolithic SiC and investigates SiC thermal stability at different high temperatures. A commercially available precursor, SMP-10, was used to synthesize stoichiometric, dense, and monolithic SiC. Thermophysical property changes during polymer to ceramic conversion were evaluated. The evolution of the phases and microstructures of the prepared SiC was studied under different pyrolysis temperatures. The fate of thus-obtained monolithic SiC and free C was studied to ultrahigh temperatures.

2. Experimental procedure

2.1. Starting materials and sample preparation

An allylhydridopolycarbosilane, commercially known as SMP-10 (Starfire Systems, Inc., NY), was used as the precursor. The molecular weight of this precursor was not well defined but believed to be > 17,000 g/mol. [24] It was a yellow liquid at room temperature. The SMP-10 polymer precursor was dissolved into toluene and stirred with a magnetic stirrer at 50 °C with a Karstedt's catalyst (0.05 wt%) in a glovebox (Ar atmosphere) for 1 h. The mixed solution was transferred into an aluminium pan and kept at 40 °C for 24 h for solvent removal (Fig. 1a). Then the aluminium pan with the precursor was heated to 120 °C for 48 h in the glovebox. The resulted sample was a translucent solid polymer, which was further shaped through a ~14.5 mm diameter gel-cutting tool (Fig. 1b). The thickness of the samples was maintained as ~3.5 mm. After that, the crosslinked samples were transferred to a vacuum furnace for curing at 250 °C for 2 h at a heating rate of 2 °C/min (Fig. 1c).

The crosslinked pellets were pyrolyzed in two steps. In the first step the crosslinked specimens were pre-pyrolyzed to 1200 °C for 2 h in an alumina tube furnace (Horizontal Tube Furnace, CM Furnaces Inc., Bloomfield, NJ) under an argon atmosphere. These pellets retained their shape after this first cycle of heating. Subsequently, the samples were placed in a graphite crucible and loaded in a graphite furnace (Oxy-Gon, New Hampshire, USA) for pyrolysis under flowing argon at temperatures from 1600 °C to 2500 °C for 1 h (Fig. 1d). The temperature control of the samples was done by measuring the temperature of the crucible surface with an optical pyrometer. The argon flow was maintained at a rate of 300 ml/min during heating and cooling. The chamber pressure was maintained at 30–50 torr during the entire heating and cooling process. The samples were labelled as SiC-XX00, where the XX in the sample codes, e.g., 1200 in SiC-1200, indicates the pyrolysis temperature of the samples, i.e., 1200 °C.

2.2. Characterization and analysis

Atomic structural changes in the polymeric network during crosslinking and pyrolysis were analyzed using Fourier transform infrared spectroscopy (FTIR, Varian 670-IR, Varian Inc., USA). The mass

loss of the crosslinked SMP-10 samples during pyrolysis was calculated by the difference between the initial and final masses of the samples. The volume changes were calculated by measuring the dimensions of the crosslinked and pyrolyzed samples using a vernier calliper. The apparent porosity and bulk density of the samples were calculated using the Archimedes' principle. After the dry weight (D) of the samples was measured with an analytical balance (Model USS-DBS8, US Solid digital analytical balance), the samples were immersed in a beaker containing deionized water and kept inside a desiccator attached to a vacuum pump. The vacuum (25 mm Hg pressure) inside the desiccator was created and maintained for 4 h so that all the open pores of the samples was filled with water. After that, the samples were taken out from the beaker and water on the sample surface was wiped out with soft tissue paper. After that, the weight of the sample was recorded in air, termed as soaked weight (W). Then, the suspended sample weight (S) was measured while the sample was immersed into deionized water with the help of a titled pan. The apparent porosity and bulk density of the samples were calculated as:

Apparentporosity (%) =
$$\frac{W - D}{W - S} \times 100$$
 (1)

BulkDensity (g/cc)

$$= \frac{D}{W - S} \times density of deionized water(g/cc)$$
 (2)

The composition analysis was performed by Galbraith Laboratories, Inc. (Knoxville, TN, USA). C and Si amounts were determined via combustion and Inductively Coupled Plasma - Atomic Emission Spectroscopy (ICP-AES) methods, respectively. Further, we assumed that any trace impurities in the samples were O. Thus, the difference in mass between the total sample and the combined mass of C and Si gave an estimate of the O content. Phase analysis was carried out by X-ray diffraction (Rigaku Ultima IV, Japan) using CuKα radiation (40 mA current, 40 kV accelerating voltage) from 10 to 80° at a scan rate and step size of 3° minute-1 and 0.03°, respectively. The phases present within the samples were identified by matching the obtained X-ray diffraction (XRD) patterns with the standard JCPDS files using X'Pert HighScore (Philips Analytical, NL) software. The SiC crystallite size at different pyrolysis temperatures was calculated using Scherrer's equation from their respective XRD spectra. Further, Raman spectra of the samples were obtained in the 1000 cm⁻¹ to 3500 cm⁻¹ spectral range by using a XploRA PLUS confocal Raman microscope (Horiba Scientific, Piscataway, NJ, USA) with an Ar laser at 532 nm wavelength and a laser power range of $1{-}2~\mu W.$ The free C (C $_{free}$) cluster size in the SiC ceramics was calculated by fitting the obtained Raman spectra with the Lorentzian function using Origin Pro 8.5 Software. The in-plane crystallite size (L_a) values of graphite was calculated using the Tuinstra-Koenig equation: [25].

$$L_a = \frac{C(\lambda)}{\frac{I_D}{I_G}} \tag{3}$$

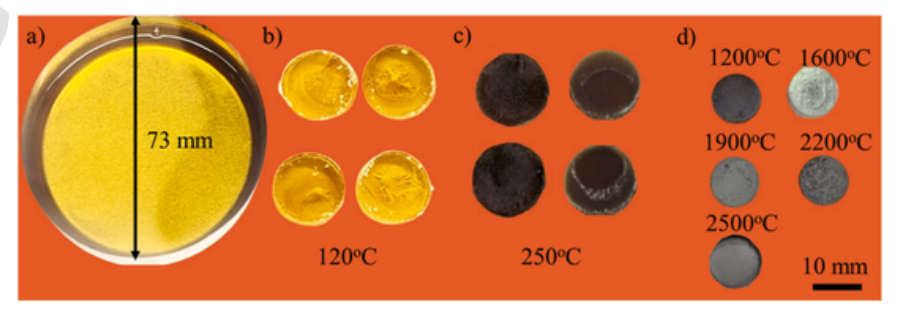


Fig. 1. Synthesis steps of monolithic SiC through gel casting of crosslinked SMP-10 followed by pyrolysis.

where the $C(\lambda)$ value for the wavelength used was 4.95 nm. The crystallite thickness (L_c)of these $C_{\rm free}$ clusters was calculated using Scherrer's equation from their respective XRD spectra.

To investigate the morphology of the SiC ceramics at high temperatures, scanning electron microscopy (SEM, JSM IT-500HR, JEOL, Tokyo, Japan) was performed on the pyrolyzed SiC pellets with a 20 kV accelerating voltage using a Schottky field emission (FEG) electron source. To understand the nanostructure evolution of SiC ceramics at different temperatures, bright field and high-resolution imaging was performed using a transmission electron microscope (STEM - ThermoFisher Titan 80/300 (FEI), USA) at an accelerating voltage of 300 kV. Powdered samples were dispersed in ethanol, ultrasonicated, and drop-cast on C coated copper grids (300 mesh, Ted Pella, USA). For analysis of the high-resolution TEM micrographs (HRTEM), DigitalMicrograph® (Gatan Ametek, USA) software was used. The lattice fringes were calculated by applying the fast Fourier transform (FFT) algorithm on selected areas over the micrograph through the Gatan Microscopy Suite Software. After computation, the fringe width was measured from the inverse FFT image derived from the micrograph.

3. Results and discussion

3.1. Thermophysical changes

The FTIR results of the 'as-received SMP-10 precursor (liquid)', crosslinked, and 1200 °C pyrolyzed samples are shown in Fig. 2. The liquid precursor (Fig. 2a) shows the following peaks: ~2915 (-CH₃ stretching), ~2850 (CH₂ stretching), ~2120 cm⁻¹ (-Si–H stretching), ~1630 cm⁻¹ (C=C stretching), ~1350 cm⁻¹ (CH₃ bending), ~1255 cm⁻¹ (Si-CH₃ stretching), ~1034 cm⁻¹ (Si-CH₂-Si stretching), ~940 cm⁻¹ (-Si–H deformation), ~820 cm⁻¹ (-Si–CH₃ wagging), and ~733 cm⁻¹ (Si–C stretching). [12,22] In the crosslinked SMP-10 sample, all the bonds remain the same except for the bond at 1630 cm⁻¹. The allyl (C=C) bond vanishes in the crosslinked sample (Fig. 2b), indicating the completion of the crosslinking reaction. The crosslinking reaction is mainly related to the addition reaction of C=C bonds of allyl (H₂C=CH-CH₂-) and -Si–H sites among the SMP-10 monomers at 250 °C. This hydrosilylation reaction results in the formation of

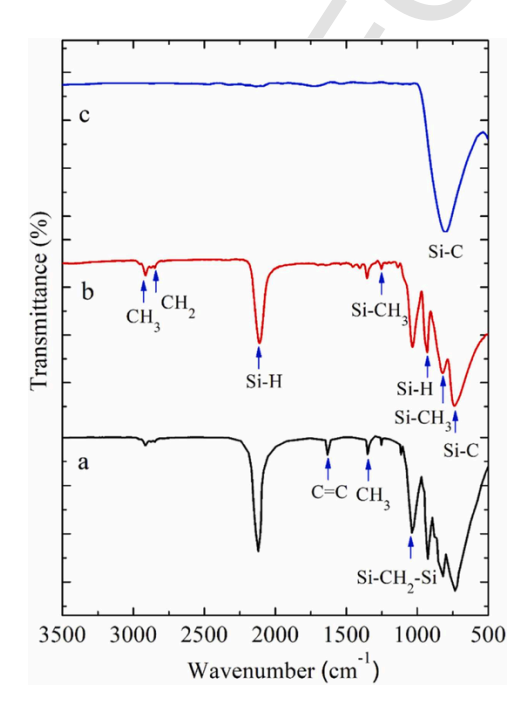


Fig. 2. FTIR spectra of (a) liquid SMP-10 precursor, (b) crosslinked at 250 $^{\circ}$ C, and (c) pyrolyzed at 1200 $^{\circ}$ C.

 ${\rm -CH_2-CH_2-CH_2-SiH(CH_2)}{\rm -}$ containing chains in the crosslinked polymers. [26] Thus, the bond intensity of -Si-H in the crosslinked SMP-10 weakens as compared to that of the SMP-10 liquid. For the pyrolyzed sample, all the H-containing bonds are absent (Fig. 2c), which confirms the complete transformation of polymer to ceramic at 1200 °C. The only absorption peak is at ~806 cm-1 wavenumber, attributed to the stretching mode of Si-C bonds. [27] It should be noted that there are no Si-O-Si bonds present in the pyrolyzed samples, which indicates negligible O contamination of the SMP-10 samples. These observations lend support to the formation of O-free SiC samples.

The physical properties of the pyrolyzed SMP-10 samples are given in Fig. 3. The mass loss is 15.00%, 16.36%, 20.63%, 26.64%, and 89.50% at 1200 °C, 1600 °C, 1900 °C, 2200 °C, and 2500 °C, respectively (Fig. 3a), which are low compared to those obtained in other studies under similar pyrolysis conditions. [12,22] The total mass loss remains low up to 2200 °C (~26.64 wt%). However, a sudden mass loss of 89.50% is observed at 2500 °C. This loss in mass is because the element with the highest atomic weight (primarily Si, since C cannot evaporate in any form from sample in an argon atmosphere) leaves the system from 2200 °C to 2500 °C. The corresponding volume shrinkages of the samples are also shown in Fig. 3a. The SMP-10 samples shrink by 53.3 vol% at 1200 °C. Moreover, pyrolysis at 1600 °C, 1900 °C, and 2200 °C causes further volume shrinkage of 56.90%, 58.34%, and 83.73%, respectively. It is surprising that further pyrolysis to 2500 °C causes expansion of the sample, and the shrinkage decreases to 68.20%. This volume expansion is believed to be due to the formation of excessive graphite. [28] The transformation from the more densely packed

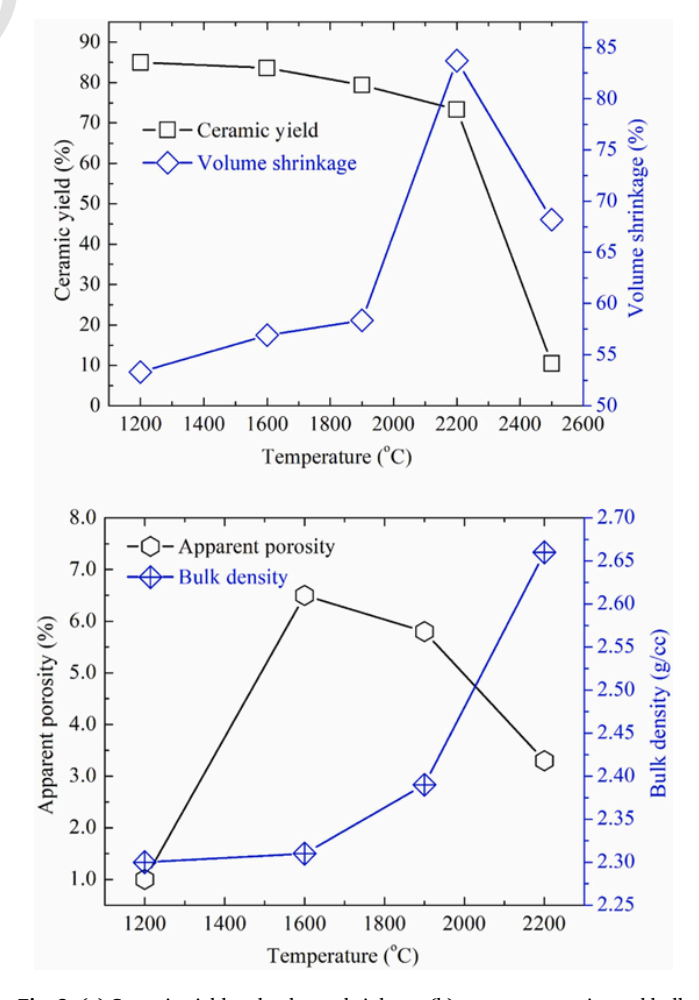


Fig. 3. (a) Ceramic yield and volume shrinkage, (b) apparent porosity and bulk density of the SMP-10 samples pyrolyzed from $1200\,^{\circ}$ C to $2500\,^{\circ}$ C.

structure of SiC to the layered structure of graphite leads to an atomic rearrangement and thus an increase in interlayer spacing, resulting in volume expansion. [29] Although the mass loss from 2200 to 2500 °C pyrolysis temperature is 62.86%, the sample volume expands by 15.53% rather than shrinking. This expansion indicates the formation of graphitic C from 2200 °C to 2500 °C and hence supports the mass loss curve in Fig. 3a. The sample is likely constituted of porous C skeletons after pyrolysis at 2500 °C.

Fig. 3b shows the apparent porosity and bulk density of the SiC samples at different pyrolysis temperatures. At 1200 °C, the porosity is < 1%. At 1600 °C, the porosity increases to 6.50%. The increase in porosity may be primarily due to the mass loss in the form of gaseous species (Fig. 3a), which eventually leaves the system by creating pores. Further, pyrolysis of the SMP-10 samples at 1900 °C to 2200 °C decreases the porosity from 6.50% to 3.30%, respectively and hence densifies the samples. The decrease in porosity is primarily due to the increase of volume shrinkage in this temperature range (Fig. 3a). The bulk densities of the SiC samples are 2.3 g·cm⁻³, 2.32 g·cm⁻³, 2.4 g·cm⁻³, and 2.7 g·cm⁻³ at 1200 °C, 1600 °C, 1900 °C, and 2200 °C, respectively. Thus, the bulk density increases by 4.40% and 17.40% at 1900 °C and 2200 °C, respectively. It should be noted that the bulk density increases despite the porosity increase. However, the porosity and bulk density of the samples pyrolyzed at 2500 °C cannot be calculated through the Archimedes method. At this temperature, there is a drastic density decrease, the samples are afloat on the water surface even after the desiccation process, which means that the sample has a lower density than water.

3.2. Phase and composition evolution

The elemental contents of Si and C are shown in Table 1. The empirical formula of the pyrolyzed samples at different temperatures are also determined (Table 1). The free C in the SiC system was calculated according to literature. [22,30–32] The SiC ceramics after pyrolysis at different temperatures contain 34.9 to 40.3 wt% C and <0.12 wt% O. These low amounts of O present are likely due to O contamination in the precursor. O exposure during synthesis and handling would lead to higher amounts of O, ranging from 3 to 6.7 wt%. [8,12,21,22,33–35] C/Si ratio and C consistently decrease with pyrolysis temperature increase up to 1900 °C. Also, the concentration of O decreases as the pyrolysis temperature increases and disappears from the sample composition above 1600 °C. The decreases in O and C are due to the removal of formed CO through carbothermal reduction of SiC(O) network to SiC.

$$\operatorname{SiC(O)}_{(s)} + \operatorname{C}_{\operatorname{free}(s)} \to \operatorname{SiC}_{(s)} + \operatorname{CO}_{(s)} \uparrow \tag{4}$$

The Si concentration increases with the pyrolysis temperature up to 1900 °C. Higher pyrolysis temperature leads to a decrease in the Si content. Thus, the SiC synthesized at 1900 °C has the highest Si content, the lowest C/Si ratio ($\sim\!1.25$), and the least amount of free C. The decrease of Si for the SiC-2200 sample is attributed to the evaporation of Si from the SiC matrix at 2200 °C. The empirical formulas indicate that the SiC samples synthesized are not stoichiometric but C-rich at all the pyrolysis temperatures. The amount of $C_{\rm free}$ is the least (6.9 wt%) for the SiC-1900 sample.

Table 1Elemental compositions and empirical formulas of SMP10-derived SiC monoliths.

Samples	Element content (wt%)			Empirical formula	C/Si
	Si	С	O		
SiC-1200	60.4	39.48	0.12	SiC _{0.9962} (O _{0.0075}) + 0.53 C _{free}	1.53
SiC-1600	60.9	39.09	0.10	$SiC_{0.9969}^{0.9962}(O_{0.0063}^{0.0075}) + 0.50 C_{free}^{1768}$	1.50
SiC-1900	65.1	34.9	0	SiC + 0.25 C	1.25
SiC-2200	59.7	40.3	0	SiC + 0.58 C _{free}	1.58

The phase evolution and crystallization results of the SiC ceramics are given in Fig. 4. The SiC ceramics are primarily amorphous at 1200 °C, with clear but broad peaks at $2\theta = 35.6^{\circ}$, 60° , and 71.8° , which are assigned to cubic β -SiC nanocrystallites; the crystallite size is \sim 1.9 nm, based on Sherrer's equation. [36-39] Further pyrolysis at 1600 °C, 1900 °C, and 2200 °C leads to stronger and sharper peaks at 35.6°, 41.4°, 60.0°, 71.8°, and 75.5°, which are assigned to the (111), (200), (220), (311), and (222) planes of β-SiC. The crystallinity and crystal growth of β -SiC increase with temperature. The crystallite size of β -SiC increases to \sim 8.9 nm and \sim 28.50 nm for the samples pyrolyzed at 1600 °C, and 1900 °C, respectively (Table 2). The nanocrystalline nature is maintained at 2200 °C while the crystallite size increases to ~39.8 nm. The drastic crystallite growth above 1600 °C is due to the decrease in free C and thus the C/Si ratio in the SiC matrix (Table 1). A small diffraction peak at $2\theta = 26^{\circ}$ is ascribed to the crystalline C present at 2200 $^{\circ}$ C. The β -SiC phase remains stable even at 2200 $^{\circ}$ C.

The X-ray diffraction pattern of the 2500 °C pyrolyzed sample shows peaks at $2\theta=26.3^\circ$, 42.7° , 44.5° , 54.4° , and 77.7° , which are indexed as the (002), (100), (004), and (110) planes of graphitic C. The disappearance of the SiC peaks indicates the disintegration of SiC at 2500 °C. The graphitic C remains as the main crystalline phase at 2500 °C.

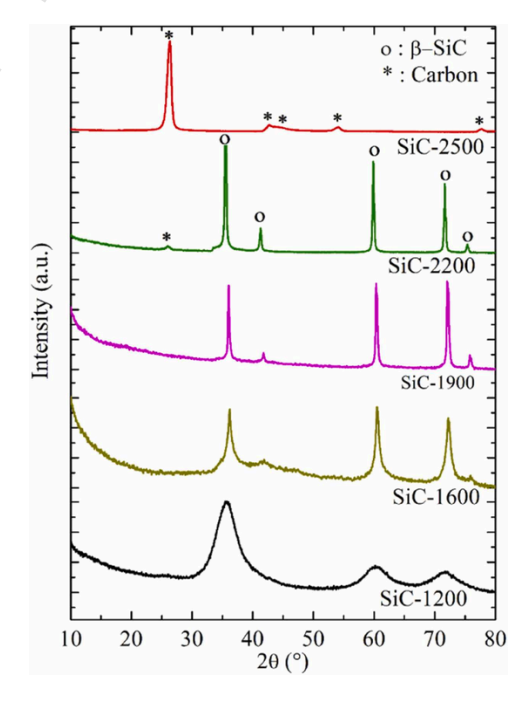


Fig. 4. X-ray diffraction patterns of the SiC samples pyrolyzed from 1200 $^{\circ}\text{C}$ to 2500 $^{\circ}\text{C}$.

Table 2 C and SiC nanocrystallite sizes at different pyrolysis temperatures.

Samples	SiC crystallite size (nm)	Raman peak position (cm ⁻¹)		I (D) I (G)	Graphitic C crystallite size (nm)	
		D	G		(L _a)	(L _c)
SiC- 1200	1.9	1342	1599	1.64	3.02	
SiC- 1600	8.9	1350	1581	0.79	6.28	
SiC- 1900	28.5	1343	1580	0.81	6.11	
SiC- 2200	39.8	1350	1583	0.11	44.55	7.1
SiC- 2500		1346	1579	0.09	55.15	9.9

The structural evolution of the free C phases in the SiC samples at different pyrolysis temperatures was studied by analyzing the Raman spectra shown in Fig. 5, and the crystallite size (L_a) was calculated using Eq. (3). The D band at 1342–1350 cm⁻¹ originates from the A₁ vibration mode of the graphite lattice defects. The G band in the range of 1579–1599 cm⁻¹ originates from the E_{2g} stretching vibration mode of the graphite lattice plane, proving the existence of graphitic C structure in the SiC samples. Moreover, the 2D band near 2700 cm⁻¹ originates from the two-phonon resonance of graphene, indicating the stacking of graphene layers. [40] With the pyrolysis temperature increase, the D band becomes weaker while the G and 2nd order Raman spectrum bands (2D, D", and 2D') gradually become sharper. This indicates the reduction of defects, crystallization enhancement, and formation of a graphene-like structure. Also, the $\frac{I_D}{I_G}$ (ratio of the intensities of the D and G bands, Table 2) values decrease with the pyrolysis temperature increase, demonstrating increased ordering or graphitization (sp² C) in the SiC samples.

The bands at 781 cm $^{-1}$ and 950 cm $^{-1}$ are attributed to the scattering peaks of the β -SiC transverse optic and longitudinal optic phonon modes. [41,42] There are obvious Raman characteristic peaks in SiC-1600 and SiC-1900. Even though SiC is not observed in the XRD pattern of the SiC-2500 sample, a vague SiC peak is present in Fig. 5 for SiC-2500, which is likely due to the presence of a low amount of SiC at 2500 °C not detectable by XRD. A Si Raman band at 520 cm $^{-1}$ for the SiC-2200 sample indicates that at 2200 °C, the Si-C bond breaks and Si leaves the SiC matrix as elemental Si. In addition, the crystallite size (L_a) of C at 1900 °C remains in the range of \sim 3 to 6.3 nm. However, the in-plane crystallite size of C rises drastically for the SiC-2200 (L_a = 44.55 nm) and SiC-2500 (55.15 nm) samples. Further, the crystallite thickness (L_c) of C at 2200 °C and 2500 °C are 7.1 nm and 9.9 nm, respectively.

3.3. Microstructure evolution

The SEM micrographs of the SiC samples pyrolyzed at different temperatures are shown in Fig. 6. The samples prepared at 1200 °C show dense and pore free microstructure (Fig. 6a), consistent with the density and porosity calculated by the Archimedes method (Fig. 3b). However, the samples pyrolyzed at higher temperatures (1600 °C and 1900 °C)

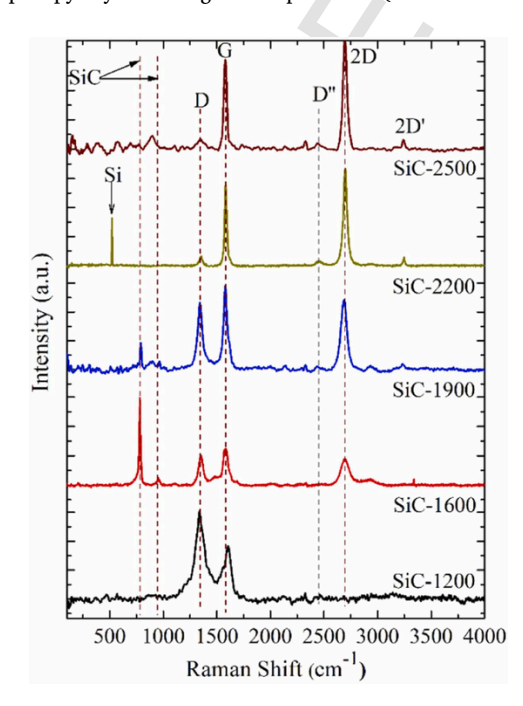


Fig. 5. Raman spectra of the pyrolyzed samples from 1200 °C to 2500 °C.

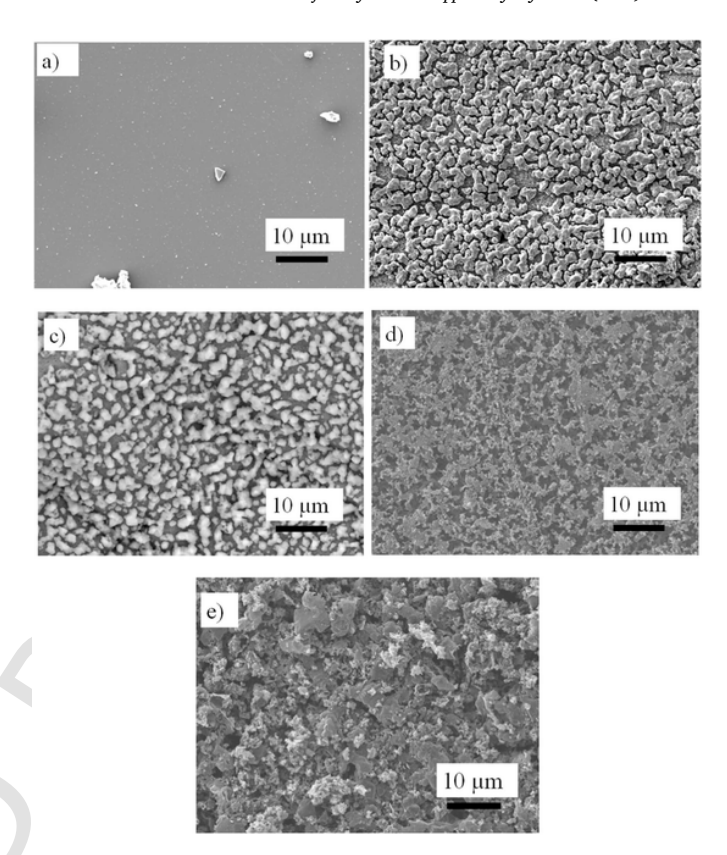


Fig. 6. SEM micrographs of the monolithic SiC samples prepared at: a) 1200 °C, b) 1600 °C, c) 1900 °C, d) 2200 °C, and e) 2500 °C.

show partially porous structures (Figs. 6b and 6c). At 1600 °C, only pores of $< 1 \mu m$ are observed (Fig. 6b). The top surface of the SMP-1600 sample is vermicular because of the formation of pits and channels throughout the SiC monolith. For the 1900 °C pyrolyzed sample, a rather diffused porous structure, with pore sizes up to a few microns, is seen (Fig. 6c). Pits and channels form because of the release of various gaseous species, such as CO and SiO, during the carbothermal reduction (Eq. 4). The bright phase on the surface is believed to be melted and solidified Si. The detail mechanism is discussed in Section 3.4. Figs. 6d and 6e show the surface morphologies of the samples pyrolyzed at 2200 and 2500 °C, respectively. The microstructure of the 2200 °C sample is highly porous (Fig. 6d) and the pore channels are uniform throughout the samples. The bright surface phase disappears. This is mainly due to the evaporation of Si from the top layer and even the interior of the SiC monolith. [43] The SiC layer beneath the top surface, which has a vermicular morphology, remains dense. After being treated at 2500 °C for 1 h, the SiC grains of the monolith mostly disappear (Fig. 6e) and the surface is converted to a porous graphitic C structure. These results are consistent with the XRD results (Fig. 4).

To understand the phase evolution and crystallization process, the TEM images of the pyrolyzed SiC specimens are shown in Fig. 7. SiC-1600 exhibits no appreciable contrast throughout the imaged area (Figs. 7a and 7b) because the nanostructure is rather homogeneous. The inverse FFT filtered image (Fig. 7b, inset 1) shows an interplanar distance of d at $\sim\!0.25$ nm, which corresponds to the interplanar spacing of the β -SiC crystalline phase and hence endorses the pseudo-crystalline nature of SiC-1600, consistent with the XRD results (Fig. 4). The crystallization of graphitic C, as seen in the Raman spectra (Fig. 5), is not observed in the TEM. However, the inverse FFT image of a selected region (inset 2, Fig. 7b) shows an interplanar distance of d at $\sim\!0.39$ nm, corresponding to the graphitic C in the SiC ceramic matrix. Due to the low volume fraction of this phase, only a few diffraction spots of graphitic C are observed (Fig. 7b), C remains mostly in the amorphous state. Some

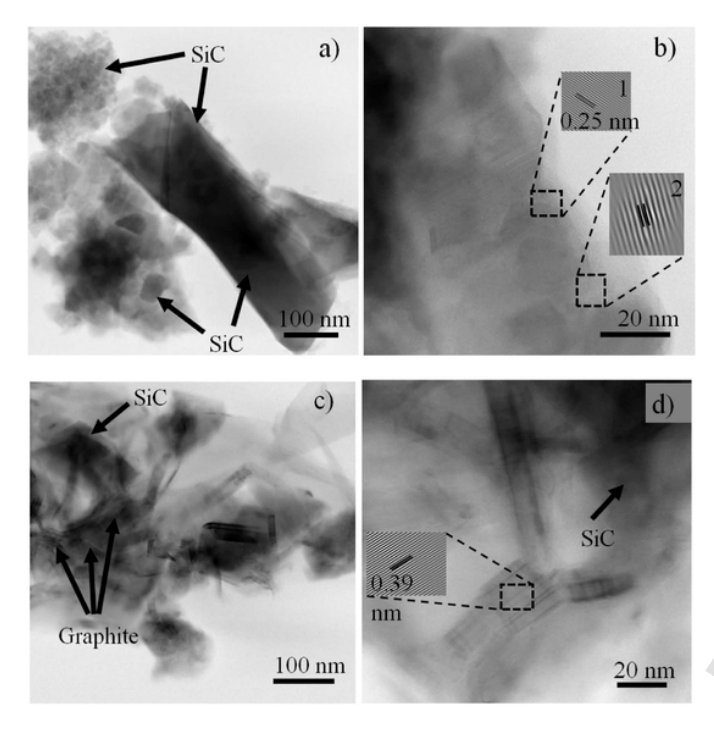


Fig. 7. (a) TEM image of 1600 °C pyrolyzed SiC, (b) HRTEM image of the SiC pyrolyzed at 1600 °C; insets 1 and 2 show inverse FFT images of the marked regions, (c) TEM image of 2200 °C pyrolyzed SiC, and (d) corresponding HRTEM image of the SiC pyrolyzed at 2200 °C; the inset shows the inverse FFT image of the marked area.

SiC crystallites remain adjacent and a few graphitic C rings are spotted on the neck/junction area of these SiC crystallites. The amorphous and lamellar C species are mainly in the exterior region of the SiC cluster. Therefore, it can be inferred that the crystalline β-SiC phases remain embedded in the amorphous C/SiC matrix. Further, these C phases can be observed in the sample pyrolyzed at 2200 °C in an abundant amount (Fig. 7c). The graphitic phase is confirmed by the inverse FFT analysis (inset image, Fig. 7d) of the marked region. The C phases are distributed all over the SiC network and the SiC crystals remain embedded in the graphite matrix. There remains empty space between graphite crystals due to SiC disintegration followed by evaporation of Si from the SiC

Fig. 8 shows the elemental distribution map of Si and C in the SiC matrix at 1600 °C and 2200 °C pyrolysis temperatures. It reveals uniform elemental presence of Si and C in the SiC matrix after pyrolysis at 1600 °C (Fig. 8a). This confirms the uniform distribution of SiC throughout the matrix. The surface region of SiC is richer in C compared to the interior of the SiC matrix. This validates the amorphous

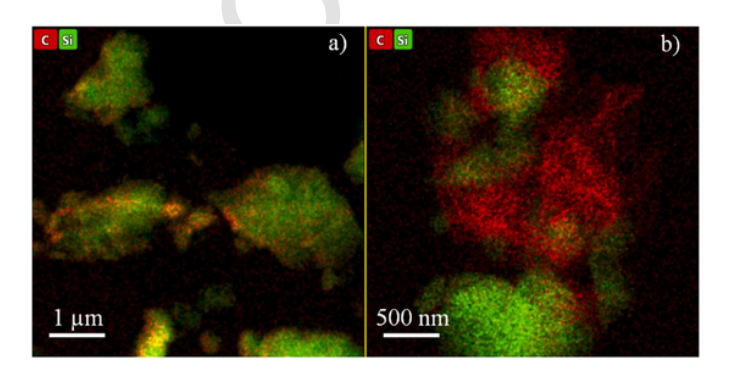


Fig. 8. Elemental maps showing Si and C distributions in (a) SiC-1600, and (b) SiC-2200 samples.

and lamellar C matrix structure around the SiC clusters as shown in Fig. 7b. For the SiC pyrolyzed at 2200 °C (Fig. 8b), Si and C have nonuniform distributions in the SiC matrix. The clusters with 'Si' persist with 'C' in the center region, confirming the presence of SiC crystals. However, C remains in excess near the neck region of the SiC crystals, the excess C bridges and encapsulates the SiC crystals in the matrix.

3.4. Fundamental understanding

As shown in Table 1, the Si content increases with temperature in the SiC samples up to 1900 °C, mainly because of C loss as CO/CO_o. This is supported by the SEM images (Fig. 6b-c, formation of micro/nano pores in the SiC monoliths due to released gases) as well as the composition changes (Table 1). As a result, the SiC pyrolyzed at 1900 °C has the lowest C and O contents, which leads to near stoichiometric SiC. Further, the Si wt% decreases at > 1900 °C pyrolysis temperature (Table 1) because the Si atoms in the SiC lattice start to evaporate. The Raman analysis of the samples shows the existence of the elemental 'Si' under 1900 °C and 2200 °C pyrolysis conditions (Fig. 5). Simultaneously, C forms in the SiC samples as evidenced by the XRD patterns (Fig. 4) and compositions of the sample pyrolyzed at 2200 °C. The XRD pattern also illustrates the disappearance of the SiC peak in the 2500 °C pyrolyzed sample, which shows no other peaks than that of graphitic C (Fig. 4). Thus, the disappearance of the SiC peaks indicates the complete disintegration of SiC at 2500 °C.

In addition, the sizes of SiC nanocrystals and the L_a of C at 2200 °C are nearly the same (Table 2). This means that the C formed in the SiC matrix is a result of C residuals after the evaporation of Si from β-SiC crystals. Literature suggests that the surface Si of β-SiC starts to evaporate at even lower temperatures (~1400 °C). [44] The probable reactions for the decomposition of SiC are as follows.

$$\beta - SiC_{(e)} \rightarrow Si_{(f)} + C_{(e)}$$

$$Si_{(f)} \rightarrow Si_{(e)}$$
(6)

$$\operatorname{Si}_{(1)} \to \operatorname{Si}_{(2)}$$
 (6)

At high temperatures, Si-C bonds gain enough thermal energy to break and become individual species (Eq. 5). Si thus forms a liquid (since the temperature is above its melting point). The metastable Si can further transition from a liquid to a vapor phase through vaporization (Eq. 6). This gaseous Si is typically monatomic and leaves the sys-

The C network forming on the surface of the SiC core as graphene sheets can be seen in the TEM images of SiC-2200 (Fig. 7c and Fig. 7d). Fig. 9 also shows a porous and flower-shaped morphology (Fig. 9a) due to the partial decomposition of SiC and evaporation of Si (marked area, Fig. 9a). Fig. 9b shows complete Si evaporation and formation of a sheet-like graphene structure at 2500 °C after SiC disintegration.

The structural evolution of the SMP-10 precursor from crosslinking to ultra-high temperatures can be illustrated in Fig. 10. It forms a disordered SiC network at 1200 °C. With further temperature increase to 1900 °C, the disordered network transforms into an ordered β -SiC structure. The disintegration of Si-C bonds and formation of graphene layers occur at 2200 °C. At 2500 °C, SiC crystals disintegrate completely, resulting in a fully layered graphene structure.

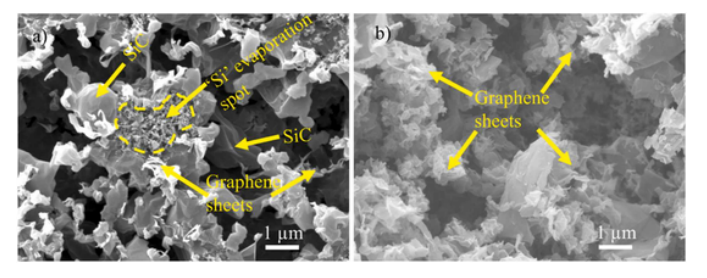


Fig. 9. SEM micrographs of SiC pyrolyzed at (a) 2200 °C, and (b) 2500 °C.

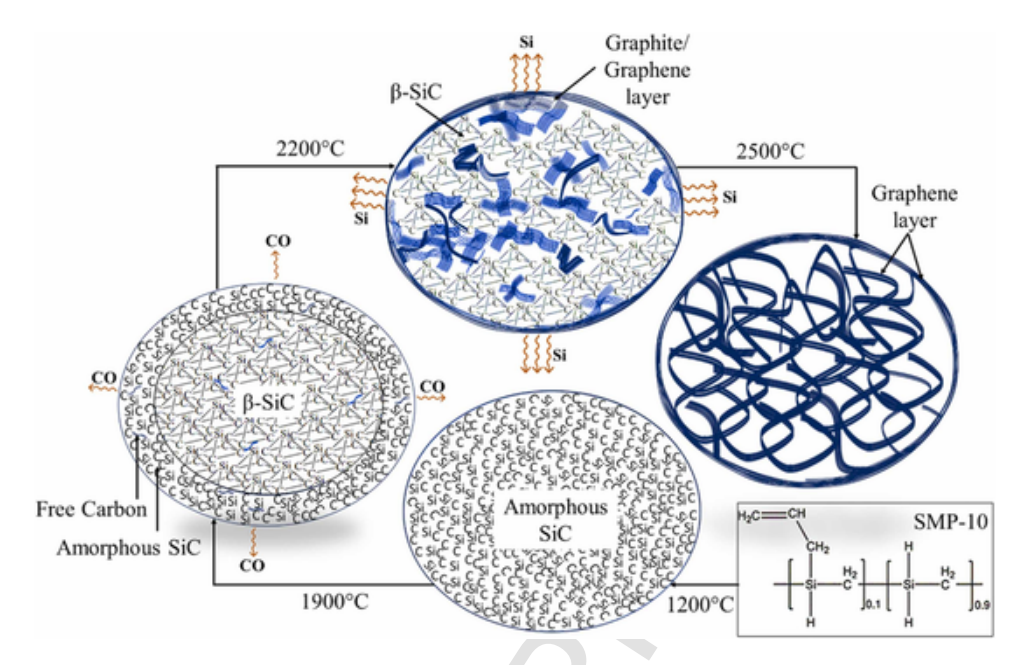


Fig. 10. A schematic demonstrating the atomic evolution of SMP-10-derived SiC.

4. Conclusions

In this study, dense SiC monolith was prepared by casting of the SMP-10 precursor followed by crosslinking and pyrolysis. The $\beta\text{-SiC}$ crystallite size was 1.9 nm at 1200 °C but grew drastically beyond 1900 °C. The SiC formed at 1900 °C was structurally dense, thermally stable, near stoichiometric and consisted of a low amount of C_{free} in the SiC matrix. Further pyrolysis at 2200 °C initiated the disintegration of ' β -SiC' and led to excessive C in the SiC matrix. The β -SiC nanocrystallites were embedded in an amorphous matrix below 1900 °C. At 2200 °C, with the evaporation of Si, the excess C encapsulated the β -SiC crystals. Pyrolysis at 2500 °C resulted in the complete disintegration of SiC due to the evaporation of "Si" from β -SiC; a highly porous structure formed. The C formed at 2500 °C had a graphene like structure. This study provides a complete map about the polymer-derived SiC monolith formation, structural evolution, and decomposition process.

Funding information

This work received financial support from the National Science Foundation under Grant No. CBET-2024546 and the Air Force Office of Scientific Research under grant number FA9550–22-1–0081.

CRediT authorship contribution statement

Lu Kathy: Conceptualization, Data curation, Formal analysis, Funding acquisition, Investigation, Methodology, Project administration, Resources, Supervision, Validation, Visualization, Writing – review & editing. **Anand Rahul:** Conceptualization, Data curation, Formal analysis, Investigation, Methodology, Validation, Visualization, Writing – original draft.

Declaration of Competing Interest

The authors declare the following financial interests/personal relationships which may be considered as potential competing interests: Kathy Lu reports financial support was provided by National Science Foundation. Kathy Lu reports financial support was provided by Air Force Office of Scientific Research. If there are other authors, they declare that they have no known competing financial interests or personal

relationships that could have appeared to influence the work reported in this paper.

Data availability

Data will be made available on request.

References

- [1] H. Abderrazak, E. Hmida, Prop. Appl. Silicon Carbide (2011) 361.
- [2] T. Maity, Y.-W. Kim, Int. J. Appl. Ceram. Technol. 19 (2022) 130.
- [3] R. Riedel, G. Mera, R. Hauser, A. Klonczynski, J. Ceram. Soc. Jpn. 114 (2006) 425.
- [4] R.M. Laine, F. Babonneau, Chem. Mater. 5 (1993) 260.
- [5] S. Yajima, J. Hayashi and M. Omori, US Patent 4052430A, 1977.
- [6] M.F. Gozzi, M.D.C. Gonĉalves, I.V.P. Yoshida, J. Mater. Sci. 34 (1999) 155.
- [7] F. Cao, D.-P. Kim, X.-D. Li, J. Mater. Chem. 12 (2002) 1213.
- [8] A.R. Puerta, E.E. Remsen, M.G. Bradley, W. Sherwood, L.G. Sneddon, Chem. Mater. 15 (2003) 478.
- [9] S. Prochazka, in Mass Transport Phenomena in Ceramics, Springer, 1975, p. 421.
- [10] K.B. Cervantes-Diaz, M. Drobek, A. Julbe, A. Ayral and J. Cambedouzou, in Membranes, 2023.
- 11] G.H. Wroblewska, E. Nold, F. Thümmler, Ceram. Int. 16 (1990) 201.
- [12] S. Kaur, R. Riedel, E. Ionescu, J. Eur. Ceram. Soc. 34 (2014) 3571.
- [13] A.B. Shelekhin, E.J. Grosgogeat, S.-T. Hwang, J. Membr. Sci. 66 (1992) 129.
- [14] S. Yajima, Y. Hasegawa, J. Hayashi, M. Iimura, J. Mater. Sci. 13 (1978) 2569.
- [15] M.J. Wild, P. Buhler, J. Mater. Sci. 33 (1998) 5441.
- [16] X. Bao, M.J. Edirisinghe, G.F. Fernando, M.J. Folkes, J. Eur. Ceram. Soc. 18 (1998) 915.
- [17] D. Pizon, L. Charpentier, R. Lucas, S. Foucaud, A. Maître, M. Balat-Pichelin, Ceram. Int. 40 (2014) 5025.
- [18] K.B. Cervantes-Diaz, M. Drobek, A. Julbe and J. Cambedouzou, in Materials, 2023.
- [19] T. Nardin, B. Gouze, J. Cambedouzou, P. Bauduin, M.W.C. Man, X. Deschanels, D. Bourgeois, D. Meyer, O. Diat, J. Mater. Chem. 3 (2015) 3082.
- [20] S.C. Zunjarrao, A. Rahman, R.P. Singh, J. Am. Ceram. Soc. 96 (2013) 1869.
- [21] G.J. Leonel, X. Guo, G. Singh, C. Gervais, A. Navrotsky, J. Am. Ceram. Soc. 106 (2023) 5086.
- [22] B. Santhosh, E. Ionescu, F. Andreolli, M. Biesuz, A. Reitz, B. Albert, G.D. Sorarù, J. Eur. Ceram. Soc. 41 (2021) 1151.
- [23] F. Delobel, S. Lemonnier, É. Barraud, J. Cambedouzou, J. Eur. Ceram. Soc. 39 (2019) 150.
- [24] Z.D. Apostolov, E.P. Heckman, T.S. Key, M.K. Cinibulk, J. Eur. Ceram. Soc. 40 (2020) 2887.
- [25] L.G. Cançado, K. Takai, T. Enoki, M. Endo, Y.A. Kim, H. Mizusaki, A. Jorio, L.N. Coelho, R. Magalhães-Paniago, M.A. Pimenta, Appl. Phys. Lett. 88 (2006) 163106
- [26] T. Miyazaki, H. Nagasawa, T. Tsuru, M. Kanezashi, J. Membr. Sci. 625 (2021) 119147.
- [27] F. Shariatmadar Tehrani, B.T. Goh, M.R. Muhamad, S.A. Rahman, J. Mater. Sci.: Mater. Electron. 24 (2013) 1361.
- [28] Y. Zhang, T. Chen, J. Chen, Q. Zhang, Y. Gou, Mater. Sci. Eng.: A 848 (2022)

143363.

- [29] S. Jayakumari, M. Tangstad, Metall. Mater. Trans. B 51 (2020) 2673.
- [30] G.D. Sorarù, G. D'Andrea, R. Campostrini, F. Babonneau, G. Mariotto, J. Am. Ceram. Soc. 78 (1995) 379.
- [31] T. Rouxel, G. Massouras, G.-D. Sorarù, J. Sol. -Gel Sci. Technol. 14 (1999) 87.
- [32] K. Bawane, D. Erb, K. Lu, J. Eur. Ceram. Soc. 39 (2019) 2846.
- [33] J. Zheng, M.J. Kramer, M. Akinc, J. Am. Ceram. Soc. 83 (2000) 2961.
- [34] S. Kaur, G. Mera, R. Riedel, E. Ionescu, J. Eur. Ceram. Soc. 36 (2016) 967.
- [35] L.V. Interrante, C.W. Whitmarsh, W. Sherwood, MRS Online Proc. Libr. (OPL) 365 (1994) 139.
- [36] P. Colombo, G. Mera, R. Riedel, G.D. Sorarù, J. Am. Ceram. Soc. 93 (2010) 1805.
- [37] R. Anand, B.B. Nayak, S.K. Behera, J. Alloy. Compd. 811 (2019) 151939.
- [38] H. Schmidt, W. Gruber, G. Borchardt, P. Gerstel, A. Müller, N. Bunjes, J. Eur.

- Ceram. Soc. 25 (2005) 227.
- [39] R. Sujith, R. Kumar, Ceram. Int. 39 (2013) 9743.
- [40] M. Endo, C. Kim, T. Karaki, T. Tamaki, Y. Nishimura, M.J. Matthews, S.D.M. Brown, M.S. Dresselhaus, Phys. Rev. B 58 (1998) 8991.
- [41] M. Wieligor, Y. Wang, T. Zerda, J. Phys.: Condens. Matter 17 (2005) 2387.
- [42] S.M. Dong, G. Chollon, C. Labrugère, M. Lahaye, A. Guette, J.L. Bruneel, M. Couzi, R. Naslain, D.L. Jiang, J. Mater. Sci. 36 (2001) 2371.
- [43] Y. Gou, H. Wang, K. Jian, J. Eur. Ceram. Soc. 37 (2017) 907.
 - H. Huang, S. Chen, A.T.S. Wee, W. Chen, in: V. Skákalová, A.B. Kaiser (Eds.), Graphene, Woodhead Publishing, 2014, p. 3.